Title

Crystal structure of cytochrome P450 NysL and the structural basis for stereo- and regio-selective oxidation of antifungal macrolides.

Journal

Journal of Biological Chemistry, 301(3)

Authors

Murarka, Vidhi Chandresh

Kim, Jenny

Lamb, David

et al.

Publication Date

2025-01-13

DOI

10.1016/j.jbc.2025.108185

Peer reviewed

JBC RESEARCH ARTICLE

Crystal structure of cytochrome P450 NysL and the structural basis for stereo- and regio-selective oxidation of antifungal macrolides

Received for publication, November 4, 2024, and in revised form, December 28, 2024 Published, Papers in Press, January 13, 2025,
https://doi.org/10.1016/j.jbc.2025.108185

Vidhi C. Murarka[1,*], Jenny S. Kim[1], David C. Lamb[2], Steven L. Kelly[2], Thomas L. Poulos[1,3,4], and Alec H. Follmer[5]

From the [1]Department of Molecular Biology and Biochemistry, University of California, Irvine, California, United States; [2]Faculty of Medicine, Health and Life Science, Institute of Life Science, Swansea University, Swansea, United Kingdom; [3]Department of Pharmaceutical Sciences, and [4]Department of Chemistry, University of California, Irvine, California, United States; [5]Department of Chemistry, University of California, Davis, California, United States

Reviewed by members of the JBC Editorial Board. Edited by Sarah E. O'Connor

NysL, a cytochrome P450 monooxygenase from the Gram-positive bacterium *Streptomyces noursei*, catalyzes the C10 hydroxylation of 10-deoxynystain to nystatin A_1, a clinically important antifungal. In this study, we present the 2.0 Å resolution crystal structure of NysL bound to nystatin A_1. The structure of this complex provides key insights into the structural elements that dictate the regio- and stereo-selective oxidation of large 20-44-membered macrolide substrates. The closely related AmphL operates on a similar 38-member macrolide but oxidizes C8 rather than C10. This difference requires that the substrate for AmphL penetrate further into the active site relative to NysL. The depth of substrate penetration is controlled by interactions between an area of the substrate binding pocket deemed the "back-wall" and the hemiketal ring of the macrolide substrate.

Fungal diseases exhibit a mortality rate of six times that of malaria and three times that of tuberculosis (1). This statistic together with the emergence of drug-resistant fungal pathogens reflects a need for the development of new therapeutics (2). Polyene macrolide antibiotics, produced by *Streptomyces* spp. and other bacteria, are highly effective antifungal agents with a broad spectrum of activities (3, 4). Amphotericin B, for example, is the last-line drug for the treatment of fungal infections. Macrolide antifungals share a conserved backbone structure, characterized by amphipathic rod-shaped molecules composed of a large hydroxylated polyene macrolactone ring, a six-membered hemiketal ring, and a mycosamine ring attached to the macrolactone *via* a glycosidic bond (5). The primary mode of action is disruption of membrane function by interaction with ergosterol in fungal cytoplasmic membranes (6, 7). However, these macrolides also exhibit a high affinity for cholesterol in human cellular cytoplasmic membranes leading to potential nephrotoxicity (4, 7, 8). Therefore, the development of more selective and efficacious analogs of these polyene macrolides represents an ongoing and important therapeutic goal. One promising approach for the generation of novel polyene macrolides is to engineer enzymes in their biosynthetic pathways to produce antifungals that exhibit increased potency and selectivity. Rational enzyme engineering requires crystal structures. Unfortunately, there are only a few crystal structures across homologous systems, a requirement for understanding what controls substrate specificity and the application of structure-based enzyme engineering to produce new antibiotics.

The biosynthetic gene clusters that produce polyene macrolides encode modular polyketide synthases that assemble the macrolactone core as well as tailoring enzymes for further functionalization (4, 5). In the biosynthesis of nystatin A_1 by the soil-dwelling bacterium *Streptomyces noursei*, the 38-membered macrolactone ring is assembled by six polyketide synthase proteins and modified by three tailoring enzymes: two cytochromes P450 (P450s), NysN and NysL, and glycosyltransferases, NysDI (9–11). The final modification of nystatin A_1 is performed by NysL, which hydroxylates 10-deoxynystatin at position C10 illustrating the impressive regioselectivity of P450s (Fig. 1) (9, 10).

The importance of C10 hydroxylation for nystatin A_1 potency as an antifungal is controversial with some suggesting it to be critical for the active transport of nystatin (12), while others conclude that the antifungal activity of nystatin A_1 is comparable to its precursor 10-deoxy nystatin (10). Despite these contrasting results, NysL presents an attractive target for future engineering efforts. As the final step in the nystatin A_1 biosynthetic pathway, enzyme engineering strategies that affect hydroxylation regioselectivity and/or alteration of epoxidation activity can be implemented without altering the outcome of downstream functionalization. Modifications in regioselectivity or epoxidation activity have been shown to significantly alter the efficacy of similar polyene macrolides, amphotericin, and pimaricin, which are functionalized by AmphL and PimD, respectively, two P450s closely related to NysL (13).

Herein, we present the 2.0 Å crystal structure of NysL in complex with its product, nystatin A_1, and provide a detailed comparison with two other similar P450s, AmphL

* For correspondence: Vidhi C. Murarka, vmurarka@uci.edu.

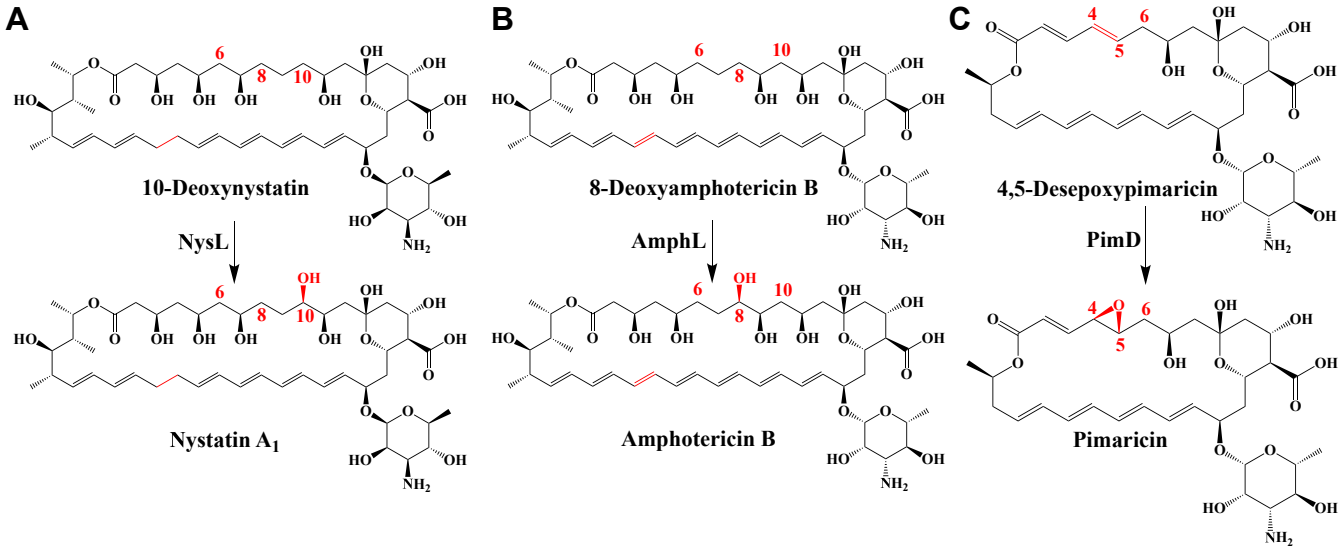

Figure 1. Reactions catalyzed by three closely related macrolide oxidizing P450s. *A*, NysL hydroxylates 10-deoxynystatin at the C10 position. *B*, AmphL hydroxylates 8-deoxyamphotericin B at the C8 position. *C*, PimD epoxidates 4,5-desepoxypimaricin across C4=C5.

and PimD, that share high sequence identity with NysL (Fig. 2) (14–16). AmphL catalyzes hydroxylation of 8-deoxyamphotericin B to give amphotericin B, also an antifungal polyene macrolide that shares the same macrolactone core as nystatin A_1 but with slight differences in conjugation and hydroxylation patterns (Fig. 1). Despite similar substrates, AmphL and NysL differentiate between the small (~2.5 Å) difference in the positioning of C8 or C10 for regio- and stereo-selective hydroxylation of their respective substrates. We also include a comparison with PimD that epoxidizes 4,5-desepoxypimaricin at the C4-C5 positions to give the 26-membered ring of pimaricin (natamycin), an antibiotic used to treat fungal infections of the eye (15).

```
NysL       -MSTPTAPPSLKAEVPPVLRLSPLLRELQSRAPVCKVRTPAGDEGWLVTRHTELKQLLHD 59
AmphL      -MVNPTPPPSLEDAAPSVLRLSPLLRELQMRAPVTKIRTPAGDEGWLVTRHAELKQLLHD 59
PimD       MTAASHDLPCLNLEPPKMLKLSPLLRALQDRGPIHRVRTPAGDEAWLVTRHAELKQLLHD 60
                    *.*:   * :*:****** ** *.*: ::********.******:*********

NysL       DRLARAHADPANAPRYVHNPFLDLLVVD-DFDLARTLHAEMRSLFTPQFSARRVMDLTPR 118
AmphL      ERLARAHADPANAPRYVKSPLMDLLIMD-DVEAARAAHAELRTLLTPQFSARRVLNMMPM 118
PimD       ERIGRTHPDPPSAAQYVRSPFLDLLISDADAESGRRQHAETRRLLTPLFSARRVLEMQPK 120
           :*:.*:* ** .* :**:.*::***: * * : .*  *** * *:** ******::: *

NysL       VEALAEGVLAHFVAQGPPADLHNDFSLPFSLSVLCALIGVPAEEQGKLIAALTKLGELDD 178
AmphL      VEGIAEQILNGFAAQEQPADLRGNFSLPYSLTVLCALIGIPLQEQGQLLAVLGEMATLND 178
PimD       VEEAADTLLDAFIAQGPPGDLHGELTVPFALTVLCEVIGVPPQRRAELTTLLAGIAKLDD 180
           **  *: :*  * **  *.**:.::::*::*:*** :**:* :.:.:* : *  :. *:*

NysL       PARVQEGQDELFGLLSGLARRKRITPEDDVISRLCLKVPSDERIGPIASGLLFAGLDSVA 238
AmphL      AESVARSQAKLFGLLTDLAGRKRAEPGDDVISRLCETVPEDERIGPIAASLLFAGLDSVA 238
PimD       REGAVRAQDDLFGYVAGLVEHKRAEPGPDIISRLNDGELTEDRVAHLAMGLLFAGLDSVA 240
              . ..* .*** ::.*. :**  *  *:****      ::*:. :* .**********

NysL       SHIDLGTVLFIQHPDQLAAALADEKLMRGAVEEILRSAKAGG--SVLPRYATADVPIGDV 296
AmphL      THVDLGVVLFTQYPDQLKEALADEKLMRSGVEEILRAAKAGGSGAALPRYATDDIEIADV 298
PimD       SIMDNGVVLLAAHPDQRAAALADPDVMARAVEEVLRTARAGGS-VLPPRYASEDMEFGGV 299
           : :* *.**:  :***   **** .:*  .***:**:*:***     ****: *: :..*

NysL       TIRAGDLVLLDFTLVNFDRTVFDEPELFDIRRAPNPHLTFGHGMWHCIGAPLARVNLRTA 356
AmphL      TIRTGDLVLLDFTLVNFDEAVFDDADLFDIRRSPNEHLTFGHGMWHCIGAPLARMMLKTA 358
PimD       TIRAGDLVLFDLGLPNFDERAFTGPEEFDAARTPNPHLTFGHGIWHCIGAPLARLELRTM 359
           ***:*****:*: * ***. .*   : **  *:** *******:**********: *:*

NysL       YTLLFTRLPGLRLVRPVEELRVLSGQLSAGLTELPVTW       394
AmphL      YTQLFTRLPGLKLASSVEELQVTSGQLNGGLTELPVTW       396
PimD       FTKLFTRLPELRPELPVEQLRLKEGQLSGGFAELRVVW       397
           :* ****** *:    **:*:: .***..*:::** *.*
```

Figure 2. Sequence alignment of NysL, AmphL, and PimD. An *asterisk* (*) denotes conserved identical amino acid, a *colon* (:) shows conservation between groups of strongly similar properties, a *period* (.) is for conservation between groups of weakly similar properties, a *space* ( ) is for non-conserved mutation, and a *hyphen* (-) is for gap in the sequence.

Results and discussion

Overall structural analysis of NysL

We have solved the 2 Å crystal structure of NysL bound to its commercially available product, nystatin A_1 (Table 1). The NysL-nystatin A_1 complex crystallizes in the P 3_1 2 1 space group and exhibits two NysL molecules in the asymmetric unit. The Cα-rms difference (Cα-RMSD) of the two molecules is 0.275 Å and the all-atom RMSD of the two nystatin A_1 molecules bound to NysL is 0.154 Å. NysL exhibits the conserved P450 triangular fold (Fig. 3*A*) with the heme iron coordinated to the protein *via* a conserved cysteine residue (Cys343) that precedes the L helix. As shown in Figure 3*B*, the carbon at position C10 of nystatin A_1 is positioned closest to the iron center with its hydroxyl group sitting 2.5 Å from the heme iron, which is consistent with the substrate being positioned for regio- and stereo-selective hydroxylation.

Substrate access channel

Structurally, AmphL (14) and PimD (15) are very similar to NysL with Cα-RMSDs of 0.632 Å and 0.868 Å, respectively. Analogous to AmphL and PimD, NysL likely uses a substrate access channel that runs parallel to the I helix (channel 2, Fig. 4) rather than the access channel near the F/G loop (channel 1) used by a majority of P450s (14, 15, 17). Channel 2 allows the macrolide substrate to enter the active site along its elongated/long axis, which requires less conformational changes/reorientation of the substrate that would be required by entry *via* channel 1 (14, 15). It is also worth noting that channel 2 forms between the I-helix and the B-C loop and is distinct from the dynamics of a secondary channel that forms between the B-C loop that is suggested to form to facilitate product egress in other P450 systems (18).

Table 1
Crystallographic data collection and refinement statistics

Parameters	NysL
PDB ID	9CV8
Wavelength	0.97946
Resolution range	37.79–2.0 (2.072–2.0)
Space group	P 3_1 2 1
Unit cell	136.29 136.29 135.6 90 90,120
Total reflections	1,111,266 (110,276)
Unique reflections	98,254 (9674)
Multiplicity	11.3 (11.3)
Completeness (%)	99.76 (99.36)
Mean I/sigma(I)	18.25 (1.65)
Wilson B-factor	35.35
R-merge	0.1727 (1.03)
R-meas	0.1809 (1.079)
R-pim	0.05345 (0.3196)
CC1/2	0.995 (0.906)
CC*	0.999 (0.975)
Reflections used in refinement	98,060 (9674)
Reflections used for R-free	4712 (455)
R-work	0.1888 (0.2861)
R-free	0.2153 (0.2915)
CC(work)	0.954 (0.692)
CC(free)	0.931 (0.620)
Number of non-hydrogen atoms	6922
macromolecules	6124
ligands	261
solvent	537
Protein residues	779
RMS(bonds)	0.008
RMS(angles)	1.06
Ramachandran favored (%)	98.32
Ramachandran allowed (%)	1.68
Ramachandran outliers (%)	0.00
Rotamer outliers (%)	1.96
Clashscore	3.22
Average B-factor	44.18
macromolecules	43.68
ligands	45.36
solvent	49.31
Number of TLS groups	8

Numbers in () are for the highest resolution shell. Statistics were generated by the "Table 1" utility in Phenix.

The "back-wall" and substrate-enzyme interactions

As shown in Figure 5, a number of hydrogen bonding (H-bonding) and nonpolar interactions between the protein and the large polyene macrolide ring help to anchor the substrate in place in NysL, AmphL, and PimD. In particular, the residues that form the "back-wall" of each enzyme's active site control how far the substrate can penetrate into the active site thereby positioning the correct carbon atom for oxidation. In NysL (Fig. 5*A*), the back-wall is defined by the residues that span from Lys277 to Leu283. Both Lys277 and Ser281 form H-bonds with the hemiketal carboxylate of nystatin A_1 while the mycosamine ring amine group forms an H-bonding interaction with the peptide carbonyl O atom of Gly280. Behind the mycosamine ring, Leu283, a part of the anti-parallel sheet β1-4, forms nonpolar contacts with the nystatin A_1 macrolactone core. Together, these interactions control how far the substrate molecule can move into the active site resulting in the optimal positioning of C10 over the heme iron for oxidation.

Catalytic residues

NysL retains the critical active site residues required for P450 O_2 activation (14, 15). In many well-studied P450s (17), the side chain of a conserved threonine in the middle of the I-helix donates an H-bond to the backbone carbonyl of an I-helix residue in the X-4 position that disrupts the helical structure. Upon dioxygen binding, this H-bond interaction is further disrupted and the active site Thr side chain is freed to form part of a proton relay network resulting in protonation of the O_2 distal oxygen required for heterolytic cleavage of the O-O bond (17) giving the competent oxidative intermediate, compound I (19). Rather than a Thr, NysL contains an active site serine, Ser236 (Ser236 in AmphL and Ser238 in PimD). A Thr at this position in all three macrolide functionalizing P450s would result in steric crowding with the substrate. As a result, these P450s use Ser, which is functionally equivalent to Thr (Fig. 6). Ser236 induces a similar disruption of the backbone helix of NysL by H-bonding with the backbone carbonyl of Ala232 that presumably breaks upon O_2 binding.

In addition to Thr or Ser, there is a highly conserved Asp residue critical in the P450 proton relay network (17). In the well-studied P450cam system, Asp251 is anchored in place through salt bridges with Arg186 and Lys178. These salt bridges are ruptured upon binding of the electron donor redox partner, putidaredoxin (Pdx), which frees Asp251 to facilitate

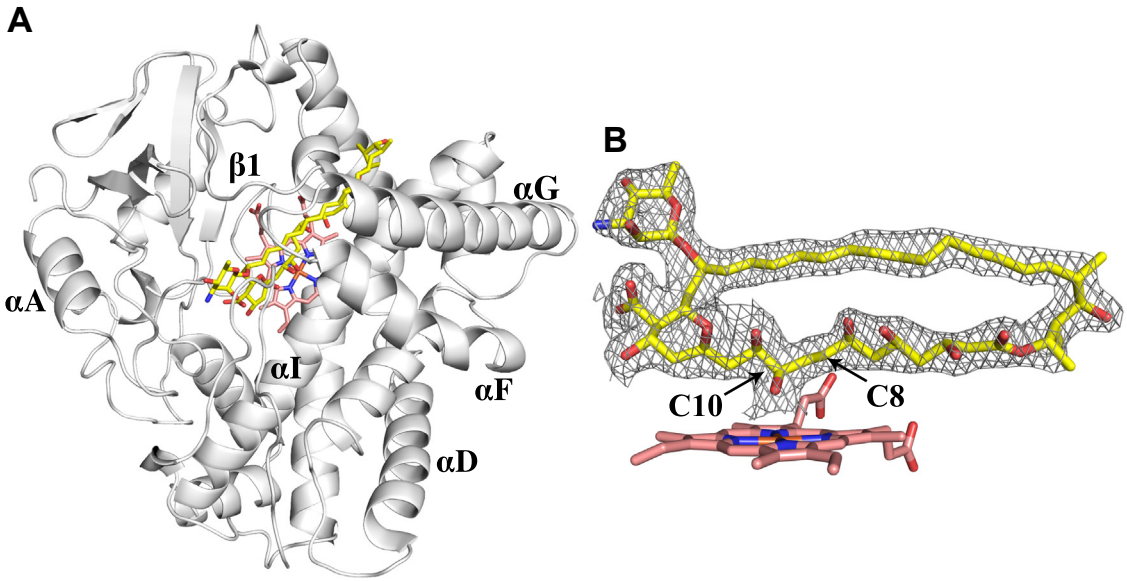

Figure 3. Structure of NysL. *A*, NysL exhibits the traditional triangular P450 fold. *B*, 2Fo-Fc electron density map contoured at 1.0 σ with nystatin A_1, the product of NysL. The C10 hydroxyl points towards the heme-iron at a distance of 3.4 Å.

the formation of a proton relay network. These functionally important structural changes are unique to Pdx binding and as a result, P450cam has a strict requirement for Pdx and no other redox partner can support P450cam catalysis (20). NysL retains the conserved Asp residue, Asp235 (Asp235 in AmphL and Asp237 in PimD) (21). However, since Asp235 does not interact with any neighboring residues, there is no need for a redox partner-mediated structural change to activate the proton relay network as in P450cam. Therefore, the NysL-catalyzed *in vitro* conversion of 10-deoxynystatin to nystatin A_1 can be supported by non-native redox partners such as spinach ferredoxin/ferredoxin reductase (10).

Comparisons of macrolide functionalizing P450s

We recently carried out a detailed structural comparison between both AmphL and PimD and concluded that subtle differences deep within the active site control the proper positioning of the large polyene macrolide ring for selective hydroxylation or oxidation (14). However, this comparison was limited by the substantial difference in the size of the substrate macrolide rings bound to these two P450s: 26 carbons in PimD and 38 in AmphL. Comparison between AmphL and NysL, which both operate on similar 38-member macrolide rings, allows for more direct analysis of the subtle differences that control regio- and stereo-selective hydroxylation.

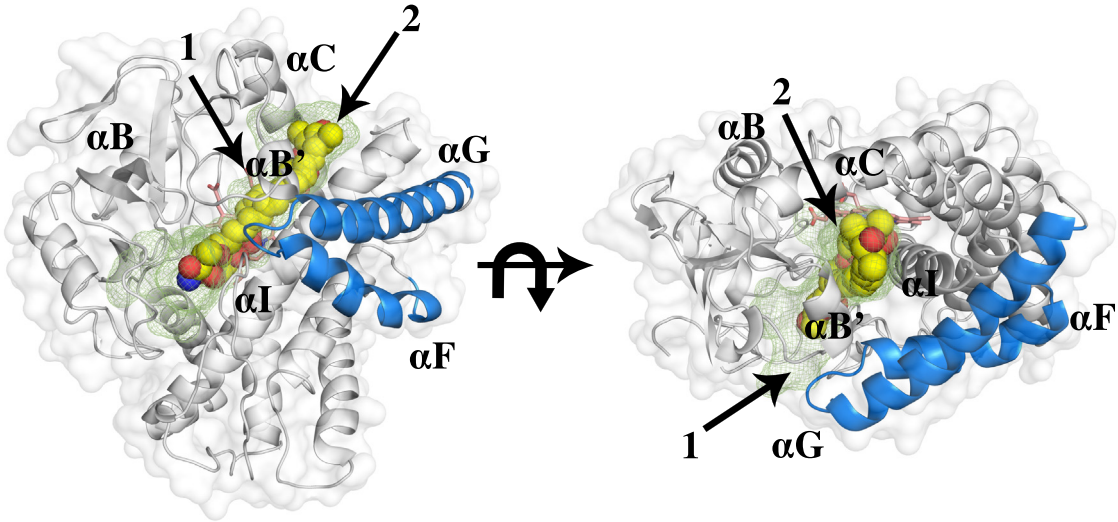

Figure 4. Potential substrate access channels of NysL. Channel 1 is located near the F/G loop and is used by the majority of P450s. In channel 1, the substrate would likely enter along its long axis requiring a ~90° rotation of the substrate and extremely large changes in the protein structure. Channel 2 (*green mesh*), parallel to helix I, is more likely the route used by NysL, AmphL, and PimD, as this channel allows the substrate to enter along the long axis requiring minimal changes in substrate orientation or protein conformation. Cavities were calculated using CavitOmiX (v, 1.0, 2022, Innophore GmbH).

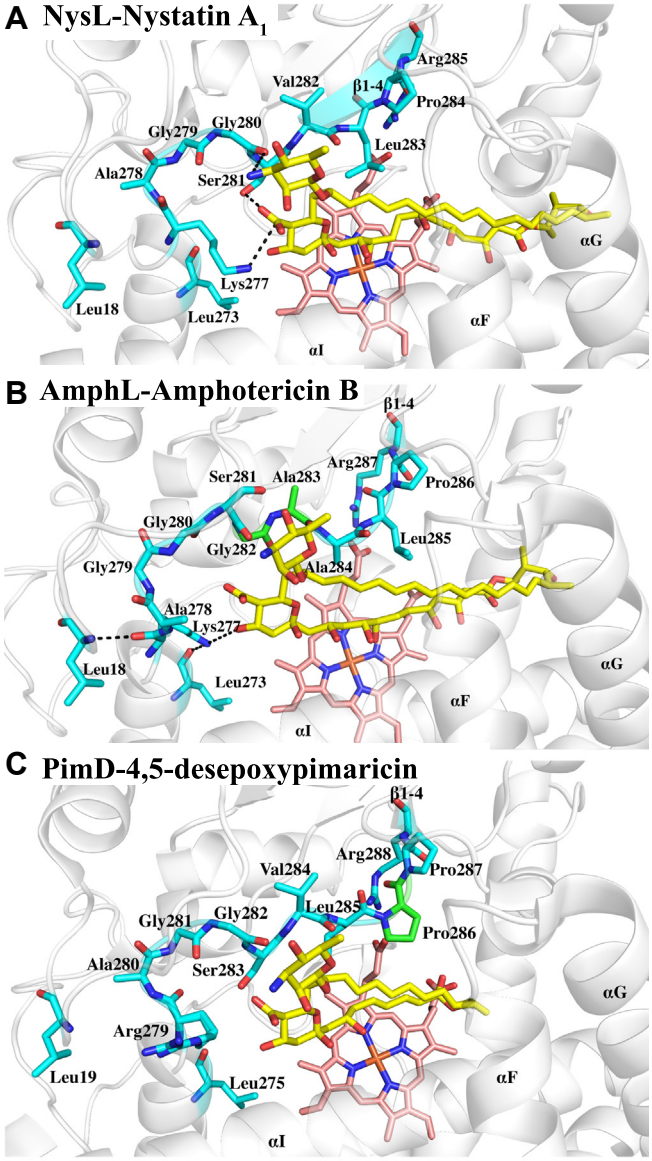

Figure 5. Substrate-P450 interactions in three closely related macrolide oxidizing P450s. The key residues involved in substrate interaction are shown in *blue* sticks, additional amino acids in the back-wall of P450s are shown in *green* sticks and H-bonds are depicted as *black dashed lines*. *A*, In NysL, Lys277 and Ser281 interact with hemiketal of nystatin A_1. The amino group of mycosamine ring of nystatin A_1 forms an H-bond with the peptide carbonyl O atom of Gly280. Leu283, part of anti-parallel β1-4, interacts with the macrolactone core of nystatin A_1. These interactions between the back-wall and nystatin A_1 position the C10 above the heme iron. *B*, In AmphL (PDB: 7SHI), there is a two amino acid insertion relative to NysL, Gly282, and Ala283, that enables the substrate to penetrate further into the active site positioning the C8 above the heme iron. This expansion is stabilized by an interaction between the peptide carbonyl O atom of Ala278 and the backbone amide group of Leu18 and a reorientation of Lys277 allowing for interaction with Leu273. There is also a partial disruption of the β1-4 sheet, which frees Leu285 to interact with the macrolactone core of the substrate. *C*, in PimD (PDB: 2XBK), there is a one amino acid residue (Pro286) insertion in the back-wall of the active site compared to NysL that shares similar implications for substrate positioning to AmphL.

Across all three systems, substrate selectivity is predominantly controlled through interactions of the hemiketal ring with residues along the "back-wall" of the active site, which we define in NysL as residues Lys277 to Leu283. The primary role played by the back-wall of the substrate binding pocket is

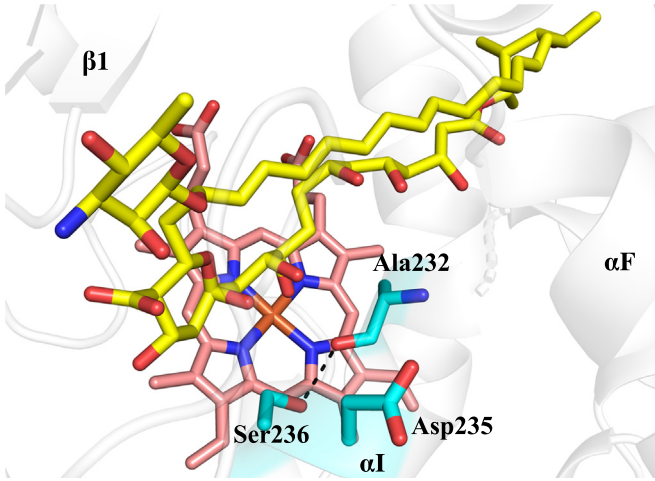

Figure 6. Catalytic residues required for O_2 activation in NysL. Ser236 in NysL is the functional equivalent of Thr252 in P450cam and donates an H-bond to Ala232. Asp235 (Asp251 in P450cam) possibly along with Ser236 in the active site is responsible for the proton relay network required for O_2 activation.

perhaps best illustrated by first comparing NysL with AmphL. While the substrates of both P450s are very similar, the substrate of AmphL can penetrate further into the active site resulting in C8 being positioned for hydroxylation rather than C10 as in NysL (Fig. 7). This is a very subtle difference given that the substrate for AmphL must slide only 2.5 Å further into the active site to properly position C8 for hydroxylation rather than C10. This difference is due to a two amino acid insertion, Gly282 and Ala283, in AmphL (Figs. 2 and 5) that expands a section of the AmphL back-wall allowing the substrate to move deeper into the active site compared to NysL. Additionally, the expansion of the back-wall of AmphL is partially stabilized by an H-bond between the peptide carbonyl oxygen atom of Ala278 and the backbone amide proton of Leu18.

As a result of this expansion, several residues of the back-wall in AmphL are in different orientations relative to NysL resulting in significant differences in substrate-protein interactions. For example, in AmphL, Ser281 points up and away from the substrate and, therefore, does not interact with the carboxyl group of the macrolide ring as in NysL. Lys277 also adopts a different orientation in AmphL relative to NysL, where it loses an H-bonding interaction with the substrate carboxyl group and instead forms an H-bond interaction with the peptide carbonyl O atom of Leu273 and the substrate hemiketal hydroxyl group. Additionally, there is a partial disruption of anti-parallel β1-4, which now starts at Arg287 in AmphL compared to Val282 in NysL. This greater flexibility frees Leu285 in AmphL to form nonpolar contacts with the polyene macrolactone core in addition to enabling the substrate to penetrate further into the active site.

Like AmphL, PimD (Fig. 5) also has an expanded back-wall owing to a single amino acid insertion, Pro286, which enables the substrate to penetrate further into the active site. As shown in Figure 7, despite the very different size of the substrate macrolactone ring, the hemiketal and mycosamine rings of the PimD and AmphL substrate nearly superimpose. These

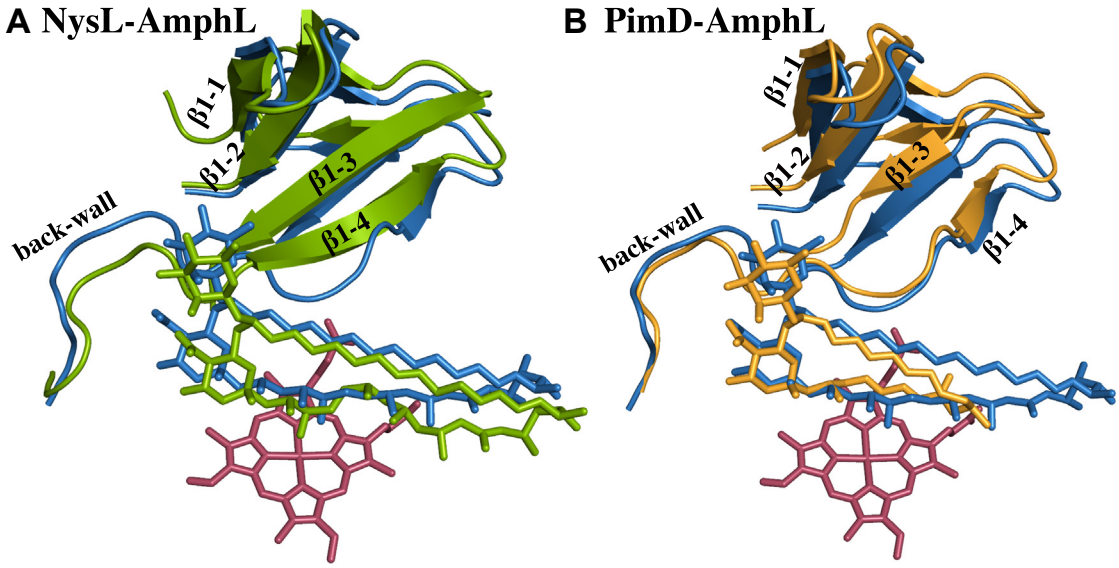

Figure 7. Structural alignment of three closely related macrolide oxidizing P450s. Alignment of (*A*) NysL-AmphL and (*B*) PimD-AmphL. AmphL is depicted in *blue*. NysL in *green* and PimD in *orange*. The heme is shown in *pink*.

structural comparisons show that the substrate binding and orientation in the active site is controlled by the interactions between the back-wall of the substrate binding pocket and the hemiketal ring of the macrolide substrate and in turn by the number of amino acid residues in the back-wall.

Conclusions

The detailed comparison of three closely related polyene macrolide oxidizing P450s, NysL, AmphL, and PimD, highlights the subtle differences in structure that lead to the precise positioning of each substrate in the active sites. Overall structural analyses of these three P450s support our hypothesis that interactions at the "back-wall" of the binding cavity with the hemiketal of the substrate is responsible for controlling how deep the substrate penetrates into the active site thereby positioning the correct carbon atom for oxidation. These interactions are, in turn, governed by the number of amino acid residues present in the back-wall. The deeper penetration in AmphL is controlled by a mere two amino acid insertion in the back-wall relative to NysL. This seemingly trivial insertion leads to expansion of the back-wall resulting in changes to the β-sheets that follow and substantial differences in substrate-protein interactions. Thus, enabling the substrate to move deeper into the active site. In addition to providing fundamental insights into the exquisite specificity of P450s, our comparisons should prove useful in structure-based engineering of macrolide processing P450s for the purpose of developing novel therapeutics.

Experimental procedures

Protein expression and purification

UniProt database was used to obtain the gene sequence that encodes NysL (Accession: Q9L4X0). A synthetic gene encoding NysL was codon optimized to express in *Escherichia coli (E. coli)* and purchased from GenScript USA Inc. The gene was subcloned using NdeI/BamHI restriction sites into a pET28a plasmid containing a thrombin-cleavable N-terminal six-His tag. The plasmid was transformed into *E. coli* BL21(DE3) cells, which were plated on Luria-Bertani (LB) agar plates containing 50 μg/ml of kanamycin. A single colony of transformed bacteria was used to inoculate 5 ml of LB media containing 50 μg/ml of kanamycin and incubated overnight at 37 °C and shaken at 200 rpm. After overnight incubation, 500 μl of overnight culture was then used to inoculate 1 L Terrific Broth (TB) media containing 50 μg/ml of kanamycin. Cultures were grown at 37 °C and shaken at 200 rpm. When the optical density (OD_{600}) of the culture reached 0.8 to 1.0, protein expression was induced following the addition of isopropyl 1-thio-D-galactopyranoside (IPTG), 1 mM final concentration, and supplemented with 30 μg/ml of δ-aminolevulinic acid (δ-ALA) to promote heme synthesis for incorporation into NysL enzyme. After induction, cells were incubated for additional 36 h at a reduced temperature of 25 °C and a shaking speed of 120 rpm and then harvested by centrifugation.

Cell pellets were suspended in lysis buffer containing 50 mM potassium phosphate (KPi), pH 7.4, 100 mM NaCl, and 5 mM imidazole and then lysed *via* sonication. The lysate was centrifuged at 15,000 rpm and 4 °C for 1 h (Beckman Coulter Avanti JA-17). The resulting supernatant was loaded onto a Ni^{2+}-nitrilotriacetate agarose column (Thermo Fisher HisPur Ni-NTA) that was pre-equilibrated with 5 column volumes (CVs) of lysis buffer. The column was then washed with 10 CVs of lysis buffer containing 15 mM imidazole. Protein was eluted using 5 CVs of lysis buffer containing 200 mM imidazole. Fractions that exhibited red color were collected and pooled. Thrombin (20 units/mg) was added to the eluted protein to cleave the N-terminal six-His tag from the protein and then dialyzed overnight against 50 mM KPi buffer (pH 7.4)

at 4 °C. Dialyzed protein was further purified by diethylaminoethyl (DEAE) anion exchange column chromatography (Cytiva) previously equilibrated with 5 CVs of 50 mM KPi buffer (pH 7.4). The column was then washed with 10 CVs of 50 mM KPi buffer (pH 7.4). Protein was eluted using a gradient of 0 to 300 mM KCl over 10 CVs. The protein fractions with Reinheitszahl purity ratio (R_z, A_{418}/A_{280}) of 1.2 and higher were pooled, and buffer exchanged into 50 mM KPi (pH 7.4) and concentrated. The protein concentration was calculated from reduced CO difference spectrum using molar extinction coefficient (ε_{450nm}) = 91 mM^{-1} cm^{-1} (22).

Crystallization, data collection, and processing

NysL crystals were grown at room temperature using the hanging drop vapor diffusion method. The reservoir solution contained 100 mM Bis-tris propane (pH 7) and 1.5 M lithium sulfate. NysL was concentrated to ∼20 mg/ml in 50 mM KPi (pH 7.4) buffer containing saturated nystatin A_1 (Sigma-Aldrich). Hanging drops were formed by mixing the protein solution with the reservoir solution in a 1:1 ratio (2 μl) and equilibrated against 700 μl of reservoir solution. Crystals were harvested and cryoprotected using ParatonN (Hampton Research) then flash frozen using liquid nitrogen. Diffraction data were collected at the Stanford Synchrotron Radiation Lightsource (SSRL) beamline 12-2. XDS was used to index, integrate, and scale the raw data (23). Phaser (24) was used to carry out molecular replacement and using PimD (PDB: 2XBK) as a search model. Refinements were carried out using phenix.refine (25) and followed by PDB_REDO (26). Data collection and refinement statistics are summarized in Table 1.

Data availability

Coordinates and structure factors have been deposited in the Protein Data Bank as entry 9CV8.

Acknowledgments—The authors thank the SSRL beamline staff for their support during remote X-ray diffraction data collection. The authors would like to thank Dr Huiying Li for helpful insights in data processing. Use of the Stanford Synchrotron Radiation Lightsource, SLAC National Accelerator Laboratory, is supported by the U.S. Department of Energy, Office of Science, Office of Basic Energy Sciences under Contract No. DE-AC02 to 76SF00515. The SSRL Structural Molecular Biology Program is supported by the DOE Office of Biological and Environmental Research, and by the National Institutes of Health (NIH), National Institute of General Medical Sciences (NIGMS, P30GM133894). The contents of this publication are solely the responsibility of the authors and do not necessarily represent the official views of NIGMS or NIH.

Author contributions—S. L. K. and V. C. M. formal analysis; T. L. P., A. H. F., V. C. M., and D. C. L. writing–review & editing; T. L. P. and V. C. M. writing–original draft; T. L. P. supervision; T. L. P., A. H. F., V. C. M., and J. S. K. investigation; T. L. P. funding acquisition; T. L. P. and D. C. L.conceptualization; A. H. F. and V. C. M. data curation. V. C. M. validation.

Funding and additional information—This work was supported by NIH grant GM131920 (T. L. P.). A. H. F. acknowledges partial support from GM120349 (Andrew S. Borovik). The contents of this publication are solely the responsibility of the authors and do not necessarily represent the official views of NIGMS or NIH.

Conflict of interest—The authors declare that they have no conflicts of interest with the contents of this article.

Abbreviations—The abbreviations used are: PdX, putidaredoxin.

References

1. Denning, D. W. (2024) Global incidence and mortality of severe fungal disease. *Lancet Infect. Dis.* **24**, e428–e438
2. Fisher, M. C., and Denning, D. W. (2023) The WHO fungal priority pathogens list as a game-changer. *Nat. Rev. Microbiol.* **21**, 211–212
3. Newman, D. J., and Cragg, G. M. (2020) Natural products as sources of new drugs over the nearly four decades from 01/1981 to 09/2019. *J. Nat. Prod.* **83**, 770–803
4. Caffrey, P., De Poire, E., Sheehan, J., and Sweeney, P. (2016) Polyene macrolide biosynthesis in streptomycetes and related bacteria: recent advances from genome sequencing and experimental studies. *Appl. Microbiol. Biotechnol.* **100**, 3893–3908
5. Aparicio, J. F., Caffrey, P., Gil, J. A., and Zotchev, S. B. (2003) Polyene antibiotic biosynthesis gene clusters. *Appl. Microbiol. Biotechnol.* **61**, 179–188
6. Bolard, J. (1986) How do the polyene macrolide antibiotics affect the cellular membrane properties? *Biochim. Biophys. Acta* **864**, 257–304
7. Byrne, B., Carmody, M., Gibson, E., Rawlings, B., and Caffrey, P. (2003) Biosynthesis of deoxyamphotericins and deoxyamphoteronolides by engineered strains of Streptomyces nodosus. *Chem. Biol.* **10**, 1215–1224
8. Zotchev, S. B. (2003) Polyene macrolide antibiotics and their applications in human therapy. *Curr. Med. Chem.* **10**, 211–223
9. Bruheim, P., Borgos, S. E., Tsan, P., Sletta, H., Ellingsen, T. E., Lancelin, J. M., *et al.* (2004) Chemical diversity of polyene macrolides produced by Streptomyces noursei ATCC 11455 and recombinant strain ERD44 with genetically altered polyketide synthase NysC. *Antimicrob. Agents Chemother.* **48**, 4120–4129
10. Volokhan, O., Sletta, H., Ellingsen, T. E., and Zotchev, S. B. (2006) Characterization of the P450 monooxygenase NysL, responsible for C-10 hydroxylation during biosynthesis of the polyene macrolide antibiotic nystatin in Streptomyces noursei. *Appl. Environ. Microbiol.* **72**, 2514–2519
11. Brautaset, T., Sekurova, O. N., Sletta, H., Ellingsen, T. E., StrLm, A. R., Valla, S., *et al.* (2000) Biosynthesis of the polyene antifungal antibiotic nystatin in Streptomyces noursei ATCC 11455: analysis of the gene cluster and deduction of the biosynthetic pathway. *Chem. Biol.* **7**, 395–403
12. Sletta, H., Borgos, S. E., Bruheim, P., Sekurova, O. N., Grasdalen, H., Aune, R., *et al.* (2005) Nystatin biosynthesis and transport: nysH and nysG genes encoding a putative ABC transporter system in Streptomyces noursei ATCC 11455 are required for efficient conversion of 10-deoxynystatin to nystatin. *Antimicrob. Agents Chemother.* **49**, 4576–4583
13. Caffrey, P., Aparicio, J. F., Malpartida, F., and Zotchev, S. B. (2008) Biosynthetic engineering of polyene macrolides towards generation of improved antifungal and antiparasitic agents. *Curr. Top Med. Chem.* **8**, 639–653
14. Amaya, J. A., Lamb, D. C., Kelly, S. L., Caffrey, P., Murarka, V. C., and Poulos, T. L. (2022) Structural analysis of P450 AmphL from Streptomyces nodosus provides insights into substrate selectivity of polyene macrolide antibiotic biosynthetic P450s. *J. Biol. Chem.* **298**, 101746
15. Kells, P. M., Ouellet, H., Santos-Aberturas, J., Aparicio, J. F., and Podust, L. M. (2010) Structure of cytochrome P450 PimD suggests epoxidation of the polyene macrolide pimaricin occurs *via* a hydroperoxoferric intermediate. *Chem. Biol.* **17**, 841–851

16. Sievers, F., Wilm, A., Dineen, D., Gibson, T. J., Karplus, K., Li, W., *et al.* (2011) Fast, scalable generation of high-quality protein multiple sequence alignments using Clustal Omega. *Mol. Syst. Biol.* **7**, 539
17. Poulos, T. L. (2014) Heme enzyme structure and function. *Chem. Rev.* **114**, 3919–3962
18. Follmer, A. H., Tripathi, S., and Poulos, T. L. (2019) Ligand and redox partner binding generates a new conformational state in cytochrome P450cam (CYP101A1). *J. Am. Chem. Soc.* **141**, 2678–2683
19. Rittle, J., and Green, M. T. (2010) Cytochrome P450 compound I: capture, characterization, and C-H bond activation kinetics. *Science* **330**, 933–937
20. Tripathi, S., Li, H., and Poulos, T. L. (2013) Structural basis for effector control and redox partner recognition in cytochrome P450. *Science* **340**, 1227–1230
21. Gerber, N. C., and Sligar, S. G. (1994) A role for Asp-251 in cytochrome P-450cam oxygen activation. *J. Biol. Chem.* **269**, 4260–4266
22. Omura, T., and Sato, R. (1964) The carbon monoxide-binding pigment of liver microsomes. I. Evidence for its hemoprotein nature. *J. Biol. Chem.* **239**, 2370–2378
23. Kabsch, W. (2010) Xds. *Acta Crystallogr. D Biol. Crystallogr.* **66**, 125–132
24. McCoy, A. J., Grosse-Kunstleve, R. W., Adams, P. D., Winn, M. D., Storoni, L. C., and Read, R. J. (2007) Phaser crystallographic software. *J. Appl. Crystallogr.* **40**, 658–674
25. Adams, P. D., Afonine, P. V., Bunkoczi, G., Chen, V. B., Echols, N., Headd, J. J., *et al.* (2011) The Phenix software for automated determination of macromolecular structures. *Methods* **55**, 94–106
26. Joosten, R. P., Long, F., Murshudov, G. N., and Perrakis, A. (2014) The PDB_REDO server for macromolecular structure model optimization. *IUCrJ* **1**, 213–220